DISEASES AND DISORDERS

miR-204–containing exosomes ameliorate GVHD-associated dry eye disease

Tian Zhou[1]†, Chang He[1]*†, Peilong Lai[2,3], Ziqi Yang[1], Yan Liu[1], Huiyi Xu[1], Xiaojing Lin[1], Biyan Ni[1], Rong Ju[1], Wei Yi[1], Lingyi Liang[1], Duanqing Pei[2]‡, Charles E. Egwuagu[4], Xialin Liu[1]*

Graft-versus-host disease (GVHD)–associated dry eye disease is characterized by extensive inflammatory destruction in the ocular surface and causes unbearable pain and visual impairment. Current treatments provide limited benefits. Here, we report that exosomes from mesenchymal stromal cells (MSC-exo) administered as eye drops notably alleviate GVHD-associated dry eye disease by suppressing inflammation and improving epithelial recovery in mice and humans. In a prospective clinical trial, 28 eyes with refractory GVHD–dry eye disease exhibited substantial relief after MSC-exo treatment, showing reduced fluorescein scores, longer tear-film breakup time, increased tear secretion, and lower OSDI scores. Mechanistically, MSC-exo reprogramed proinflammatory M1 macrophages toward the immunosuppressive M2 via miR-204–mediated targeting of the IL-6/IL-6R/Stat3 pathway. Blockade of miR-204 abolished the effects of MSC-exo, while overloading L929-exo with miR-204 markedly attenuated dry eye. Thus, this study suggests that MSC-exo are efficacious in treating GVHD-associated dry eye disease and highlights miR-204 as a potential therapeutic agent.

INTRODUCTION

Dry eye disease is the most common ocular condition that develops in a substantial percentage of patients after allo-hematopoietic stem cell transplantation as part of chronic graft-versus-host disease (GVHD) (*1*). During the process of GVHD-associated dry eye disease, the interaction of donor T cell and host antigen-presenting cells leads to the activation of donor CD8 and CD4 T cells that can attack hematopoietic tissue and/or the ocular epithelial tissues including the cornea, conjunctiva, and lacrimal gland (*2*, *3*), inducing extensive inflammatory destruction (*2*, *4*, *5*). While the infiltrated T cells from the donor, which has been demonstrated with green fluorescent protein labeling by one study (*4*), play predominant roles in the process, the recipient T cells such as the special innate-like γδ T cells may also be involved by contributing to the activation and recruitment of donor T cells (*6*). From research on rodent models (*2*, *5*) and patients (*7*–*10*), macrophages interact closely with donor T cells (*11*) and mediate the inflammatory cytokine release, orchestrating the disordered immune microenvironment of ocular surface. These activated immune cells acted as major sources of cytotoxic cytokines (*5*, *12*) and led to apoptotic cell death and deteriorated ocular tissue damage and, in severe cases, resulted in lacrimal gland fibrosis, formation of conjunctival pseudomembrane, or corneal ulcer (*13*–*15*). This disease is characterized by irritation, pain, and refractory visual impairment and severely affects the patients' quality of life, but the efficacy of current clinical drugs including tear supplements, steroid, and nonspecific immunosuppressants, or surgical intervention such as superficial epithelial debridement, amniotic membrane transplantation, or penetrating keratoplasty in extremely severe cases remains limited (*16*). Some severe patients fail to respond to these available treatments and have no other therapeutic options (*7*, *14*). It is thus the impetus to develop more efficacious immunotherapeutic agents and biologics for this devastating disease.

Mesenchymal stromal cells (MSCs) are characterized by their immunomodulatory functions that confer benefits in many human diseases (*17*). Over recent years, many studies suggest that the immunomodulatory functions of MSCs derive mostly from the paracrine effects of exosomes secreted by MSCs (MSC-exo) (*18*). Exosomes, 30- to 150-nm nanosized extracellular vesicles, contain bioactive molecules [proteins, RNA, and microRNAs (miRNAs)] that are surrounded and protected from degradation by a lipid bilayer (*19*, *20*). The lipid compatibility and relatively small size of exosomes make them suitable for delivering immunoregulatory molecules across biological barriers (*21*). Besides, unlike transplanted stem cells, exosomes lack the ability to self-replicate, thus eliminating the concerns for potential tumor formation (*22*). It was therefore of interest to investigate whether MSC-exo therapy would be effective for relieving GVHD-associated dry eye disease because of its characteristic of immunomodulatory function and advantages in clinical application. The better safety profile and increasing preference of MSC-exo over MSC therapy are reflected by 18 recent clinical trials registered at https://clinicaltrials.gov/, which recruited participants for therapeutic use of exosomes or extracellular vesicles from MSCs. Some trials showed the promising therapeutic efficacy of exosomes without any topical or systemic side effects within 24 months (*23*).

In this study, we established two dry eye mouse models and conducted a clinical study (NCT04213248) to evaluate the tolerability and efficacy of MSC-exo eye drops for treating GVHD-associated dry eye disease in patients who were refractory to currently available drugs or surgeries. In both mice and patients, MSC-exo eye drops notably restored ocular surface immune homeostasis and ameliorated inflammatory injuries in dry eye disease. The two dry eye mouse models also provided mechanistic insights into the effects of

[1]State Key Laboratory of Ophthalmology, Zhongshan Ophthalmic Center, Sun Yat-Sen University, Guangzhou 510060, P. R. China. [2]Guangzhou Institutes of Biomedicine and Health, University of Chinese Academy of Sciences, Chinese Academy of Sciences, Guangzhou 510530, P. R. China. [3]Department of Hematology, Guangdong Provincial People's Hospital, Guangdong Academy of Medical Sciences, Guangzhou 510080, P. R. China. [4]Molecular Immunology Section, Laboratory of Immunology, National Eye Institute (NEI), National Institutes of Health (NIH), Bethesda, MD, USA.
*Corresponding author. Email: liuxl28@mail.sysu.edu.cn (X.L.); hech33@mail.sysu.edu.cn (C.H.)
†These authors contributed equally to this work.
‡Present address: No. 18 Shilongshan Road Cloud Town, Xihu District, 310024 Hangzhou, Zhejiang, P. R. China.

MSC-exo in GVHD-associated dry eye disease, showing that a miRNA, miR-204, is the primary immunomodulatory cargo in the MSC-exo. More precisely, miR-204 directly targeted interleukin-6 receptor (IL-6R) to suppress the activation of IL-6/IL-6R/Stat3 pathway, inducing the inflammatory M1 macrophages to shift toward the immunosuppressive M2 phenotype in the ocular surface.

RESULTS

MSC-exo suppress dry eye in the BAC-induced mice

To examine whether MSC-exo would be an effective therapy for GVHD-associated dry eye disease, we used a widely used mouse model of dry eye induced by benzalkonium chloride (BAC), which shares essential clinical features with the dry eye disease in humans and is stable and suitable for the evaluation of treatment response (*24*, *25*). The exosomes derived from mouse bone marrow MSCs (BM-MSCs) or L929 fibroblast cells, which are usually used as controls for MSCs, were prepared and characterized by standard procedures (fig. S1, A to D). MSC-exo eye drops were formulated at 0.5×10^{10}, 2.5×10^{10}, or 12.5×10^{10} particles/ml in 5 μl per drop (*26*). When administrated twice a day for 7 days, the 2.5×10^{10} particles/ml formulation was the most optimal and effective dose and was used for further study (fig. S2, A to C). BAC-induced dry eye mice that were treated with phosphate-buffered saline (PBS) or L929-exo developed corneal edema and showed reduced transparency with extensive corneal epithelium defects (detected by fluorescein staining), while the MSC-exo–treated dry eye mice presented transparent cornea with less fluorescein staining in comparison to both groups of PBS-treated or L929-exo–treated BAC mice (Fig. 1, A and B). The secretion of tear fluid, determined by the cotton thread test, showed marked reduction of tears in BAC mice treated with PBS or L929-exo in comparison to normal mice without dry eye disease (Fig. 1C). In contrast, the MSC-exo–treated dry eye mice had increased tear secretion (Fig. 1C and data file S1), indicating the potential efficacy of MSC-exo in alleviating dry eye in BAC-induced mice. However, note that preservative-free artificial tears, which are commercial 0.3% sodium hyaluronate and are clinically used to treat dry eye disease, could not preserve the corneal epithelium or increase tear secretion in these mice (Fig. 1, A to C).

MSC-exo alleviate dry eye symptoms in NCG-GVHD mouse model

Next, we used the nonobese diabetic (NOD)–Prkdc^{em26Cd52} IL2rg^{em26Cd22} Nju (NCG)–GVHD mice, another well-established mouse model of GVHD-associated dry eye disease, to assess the efficacy of MSC-exo. The NCG mice lacked functional T cells, B cells, and natural killer cells, and the stable engraftment of human peripheral blood mononuclear cells (PBMCs) into the recipient NCG mice (hPBMCs-NCG) induced

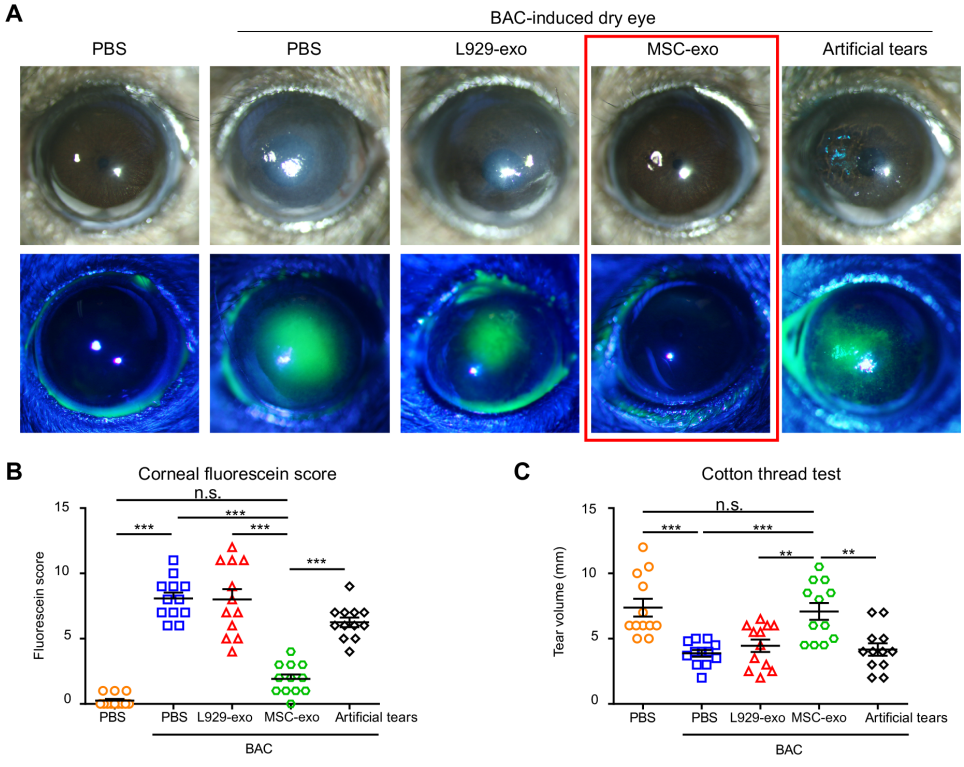

Fig. 1. Topical administration of MSC-exo alleviated dry eye symptoms in BAC-stimulated mice. (**A**) Representative images of slit lamp and fluorescein staining showing severe corneal edema and obvious epithelial defects (detected by fluorescein staining) in the eyes of BAC-stimulated mice treated with L929-exo or PBS. In contrast, BAC-stimulated mice treated with MSC-exo eye drops presented with transparent cornea and reduced fluorescein staining areas, similar to the PBS-control normal mouse eye. Unexpectedly, mice treated with artificial tears did not show similar reduction of corneal edema and epithelial defects. (**B**) Fluorescein staining scores of BAC-stimulated mice after treatment with MSC-exo or L929-exo. $n = 12$ mice, one-way ANOVA and Tukey's post hoc test. (**C**) Cotton thread test showed substantially increased tear volume in BAC-stimulated mice treated with MSC-exo compared to PBS-, L929-exo–, or artificial tear–treated BAC mice. $n = 12$ mice, one-way ANOVA and Tukey's post hoc test. n.s., not significant. $^{**}P < 0.01$ and $^{***}P < 0.001$.

clinical symptoms that resemble human GVHD (*27*, *28*). As shown in Fig. 2A, NCG-GVHD mice treated with L929-exo suffered corneal edema, decreased corneal transparency, and severe extent of corneal epithelium defects, which were revealed by intense fluorescein staining throughout the entire cornea. In contrast, mice that received MSC-exo eye drops were partially protected from GVHD-associated dry eye disease with lower fluorescent scores and elevated tear volumes (Fig. 2, A to C). Again, the artificial tear treatment was less effective with similar tear volume as mice treated with L929-exo, further underscoring the therapeutic potential of MSC-exo in both mouse models of GVHD-associated dry eye disease.

Topical MSC-exo therapy suppresses human refractory GVHD–associated dry eye disease

Fourteen patients (28 eyes) with refractory GVHD–associated dry eye disease were enrolled in a clinical trial (NCT04213248) to investigate whether MSC-exo can be used to treat dry eye disease in humans. Exosomes were derived from human umbilical cord MSCs (UC-MSC-exo) and manufactured as eye drops after modulating the osmotic pressure and pH index (fig. S1, A, E, and F). UC-MSC-exo were dispensed in 10 μg/50 μl and administrated four times a day per eye for 2 weeks. All 28 enrolled eyes of the patients with refractory GVHD–associated dry eye disease had no response to topical steroid, artificial tears, or even autologous serum. Clinical symptoms of dry eye were monitored, and representative images under white light or cobalt blue filters were taken 14 days after initiation of treatment with MSC-exo eye drops. The results revealed marked reduction in corneal epithelial damage and improvement of epithelial recovery detected by fluorescein staining [day 0 (D0) versus D14: 9.32 ± 0.64 versus 3.43 ± 0.35, $P < 0.0001$] (Fig. 3A). The relevant information and symptomatic description of the patients are provided (Fig. 3B, table S2, and data file S2). Fluorescein scores, tear-film breakup time, and Schirmer's test of each eye were analyzed on days 7 and 14. After the treatment with MSC-exo eye drops, most patients exhibited reduced fluorescein scores, longer tear-film breakup time (D0 versus D14: 1.23 ± 0.33 versus 2.85 ± 0.46, $P < 0.0001$), increased tear secretion (D0 versus D14: 2.50 ± 0.42 versus 4.68 ± 0.73, $P = 0.0176$), and lower ocular surface disease index (OSDI) scores (D0 versus D14: 50.93 ± 7.30 versus 21.76 ± 4.55, $P = 0.0002$) (Fig. 3, C to F). The dry eye symptoms including sting, burn, crust, or redness were relieved after MSC-exo treatment. No obvious impact on intraocular pressure was observed, and no complications relevant to MSC-exo were reported in these patients (Fig. 3G). Some patients could reduce the use of original drugs after the relief of dry eye symptoms. The remarkable remission of dry eye symptoms correlated with the improvement of quality of life (Fig. 3, A to F). Together, these observations suggest that MSC-exo eye drop treatment is a safe, noninvasive, and efficient cell-free therapy for patients with GVHD-associated severe dry eye.

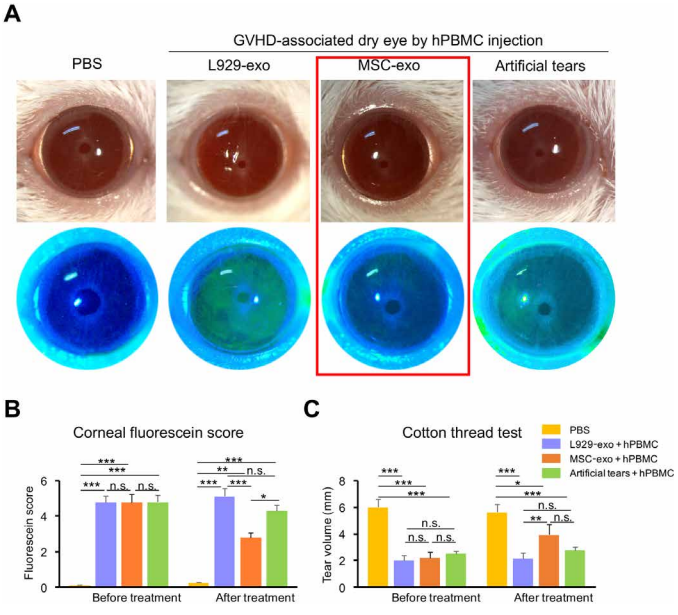

Fig. 2. The GVHD-associated dry eye disease was recovered by MSC-exo eye drops. (**A**) Slit lamp and fluorescein staining showing the representative ocular changes of hPBMC-induced GVHD in mice. The extensive epithelial defects were observed in the eyes of GVHD mice treated with L929-exo, while the MSC-exo eye drop group presented with reduced fluorescein staining areas. (**B**) The equal fluorescein staining scores in the experiment groups before any treatments indicate the baseline. After MSC-exo treatment, the score notably decreased, while there were no statistical differences between artificial tears and L929-exo. $n = 8$ mice, one-way ANOVA and Tukey's post hoc test. (**C**) MSC-exo, but not artificial tear treatment, could increase tear volume. $n = 8$ mice, one-way ANOVA and Tukey's post hoc test. $^{*}P < 0.05$, $^{**}P < 0.01$, and $^{***}P < 0.001$.

MSC-exo mediate ocular surface repair and relief of corneal inflammation

At the setting of dry eye, the ocular surface suffers from extensive inflammatory destruction. Histological analysis revealed that, in contrast to mice treated with PBS or L929-exo, MSC-exo treatment prevented corneal epithelium degeneration, increased the thickness of the central cornea and epithelium layer, and restored the well-organized corneal structure (Fig. 4A and fig. S3A). A similar epithelium protection effect was also observed in conjunctiva and lacrimal gland (fig. S4, A and B). Immunohistochemical analysis revealed that MSC-exo inhibited terminal deoxynucleotidyl transferase-mediated deoxyuridine triphosphate nick end labeling positive ($TUNEL^{+}$) cellular apoptosis while it increased the proliferative responses of $Ki67^{+}$ corneal epithelial cells (Fig. 4B and fig. S3B). The protective effects of MSC-exo were also correlated with the reduced amounts of $CD11b^{+}$ macrophages that infiltrated the cornea. The down-regulation of proinflammatory genes including *Il-6*, *Il-1*β, *Il-17a*, and *Cd86* was found in the cornea and conjunctiva (Fig. 4C and figs. S3C and S4C). These observations suggested that MSC-exo preserved corneal structures by suppressing ocular surface inflammation during dry eye.

MSC-exo reprogram ocular surface M1 macrophages into M2 phenotype

Macrophage-mediated inflammatory responses, which result in epithelial cell injuries and/or degeneration, have been considered to play a crucial role in dry eye disease (*29*). We therefore used the BAC mouse model to investigate whether the capacity of MSC-exo to suppress pathological changes that cause dry eye disease is attributable to the effects of MSC-exo on corneal macrophages. First, we labeled the MSC-exo by transfecting the MSCs with CD9-Tdtomato fusion gene and administered the CD9-Tdtomato–MSC-exo as eye drops to BAC-stimulated mice. Immunohistochemical analysis revealed the colocalization of CD9-Tdtomato–MSC-exo and $CD11b^{+}$ macrophages on corneal whole mounts of the BAC mice, indicating that macrophages infiltrating the corneal stromal layer during dry eye disease were probably the potential targets of MSC-exo therapy (Fig. 5A).

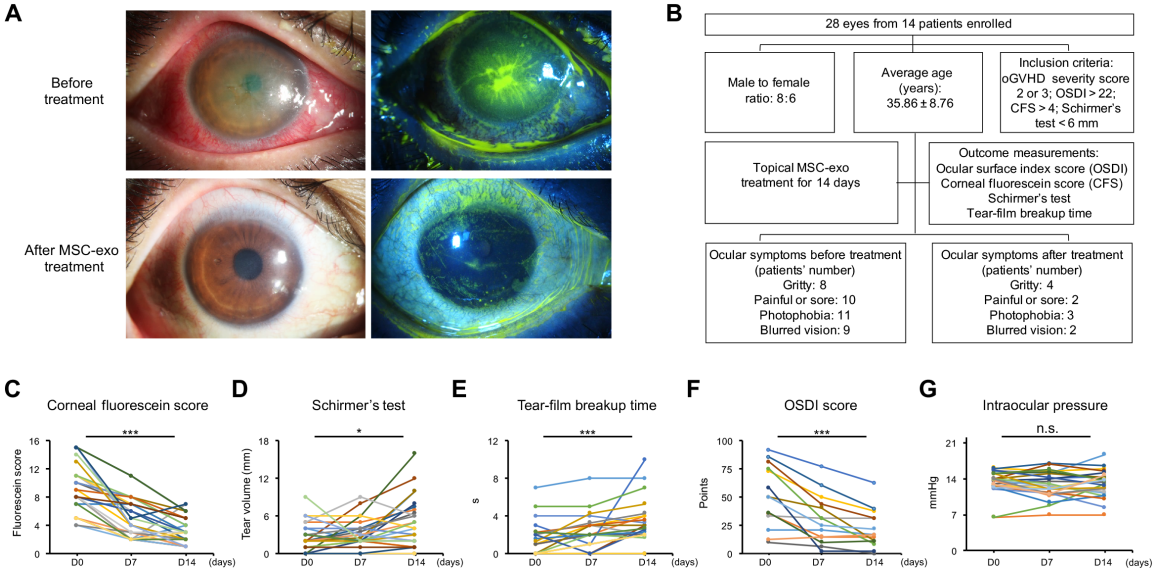

Fig. 3. MSC-exo suppressed dry eye symptoms in patients with GVHD-associated dry eye disease. (**A**) Representative images of ocular anterior segment under slit lamp and fluorescein examination before and 14 days after MSC-exo treatment. All 28 enrolled eyes with refractory GVHD–associated dry eye disease had no response to topical steroid, artificial tears, or even autologous serum. After MSC-exo eye drop usage, dry eye symptoms and pink eye were alleviated, and the cornea was more transparent with less punctate erosion areas, indicating that MSC-exo can exert a potent antixerophthalmic effect in humans. (**B**) The relevant information and symptom descriptions of the enrolled patients. (**C**) Fluorescein scores of individual eye with MSC-exo treatment at D0 and D14 showed decreased trend of fluorescein score in all eyes. (**D**) After 14-day usage of MSC-exo eye drops, more than half of the enrolled eyes presented with increased tear volume by Schirmer's test. (**E**) More stable tear film was observed after MSC-exo treatment with increased tear-film breakup time. (**F**) Except for two patients, the others reported amelioration of dryness symptoms and improved quality of life, as reflected by decreased OSDI scores after MSC-exo treatment. (**G**) MSC-exo treatment played no obvious impacts on intraocular pressure. (C to G) $n = 28$ eyes (14 patients), paired Student's t tests. $^{*}P < 0.05$ and $^{***}P < 0.001$.

Next, since the conversion of proinflammatory (M1) macrophages into the anti-inflammatory M2 phenotype correlated with wound healing and tissue regeneration (*30*, *31*), we examined the M1/M2 status upon the exosome treatments. As shown in Fig. 5 (B and C), although the dominant macrophage subset infiltrating the BAC-induced dry eye cornea treated with PBS or L929-exo remained to be $CD86^{+}CD11b^{+}CD11c^{-}$ M1 type, their proportion notably decreased in mice treated with MSC-exo. On the other hand, the levels of the anti-inflammatory $CD206^{+}CD11b^{+}CD11c^{-}$ M2 macrophages were very low in the controls but increased markedly in the MSC-exo treatment group (Fig. 5C). Application of H_2O_2 was used to induce oxidative stress to mimic the dry eye insults (*32*). It could polarize the macrophage cell line raw264.7 into the M1 phenotype. As expected, MSC-exo treatment led to notably decreased expression of M1 macrophage marker (CD86) with concomitant increase of Arg1 and CD206, two classic M2 markers (Fig. 5, D and E), suggesting that MSC-exo treatment was able to convert M1 macrophages into the anti-inflammatory M2 phenotype.

miR-204 is required for antixerophthalmic effect of MSC-exo

Exosomes contain miRNAs, and the transfer of exosomal miRNAs is emerging as a novel signaling intermediate that can be used to regulate the function(s) of a recipient cell (*33*). To investigate whether MSC-exo contain miRNAs that might contribute to its regulatory functions, we analyzed miRNAs in MSC-exo or L929-exo and identified miR-204-5p, a master regulator of ocular development (*34*–*36*), as one of the most abundant miRNAs in MSC-exo (Fig. 6, A to C). The high level of miR-204-5p expression was further verified by quantitative polymerase chain reaction (qPCR) using RNA isolated from MSC-exo–treated dry eye cornea (Fig. 6D). To further examine the key role of miRNA-204, we would like to perform the loss-of-function experiment. Since miRNA-204 is required for the survival and stability of MSCs, which precluded investigating its function during dry eye disease by knocking down miRNA-204 in MSCs, alternatively, we therefore pretreated the BAC mice with antisense oligonucleotides of mouse miR-204 (antagomiR-204) by subconjunctival injection, and this was followed by the administration of MSC-exo eye drops. The MSC-exo + antagomiR-204 group developed a full-blown dry eye disease, while the MSC-exo + antagomiR negative control (antagomiR-NC) group developed only mild dry eye symptoms, indicating that miR-204 blockage abolished the therapeutic effects of MSC-exo (fig. S5, A to C).

Moreover, we also transfected L929 cells with miR-204 precursor and demonstrated the overexpression of pre–miR-204 and mature miR-204 (fig. S6, A to C). Eye drops containing purified L929-miR-204-exo were used to treat BAC-induced dry eye mice. As shown in Fig. 6E and fig. S6D, L929-miR-204-exo treatment displayed remarkably similar therapeutic effects as the MSC-exo group, providing suggestive evidence that MSC-exo mediate their therapeutic effects on dry eye disease through miR-204.

miR-204 reprograms M1 macrophages toward M2 by targeting IL-6R

miR-204 is involved in multiple biological functions and diseases such as eye development, cancers, and diabetes by targeting many critical genes, particularly regulating the function of tumor-associated macrophages (*37*). This led us to investigate whether miR-204 might also determine the differentiation of macrophages that infiltrate the cornea during dry eye disease by targeting specific pathways in the

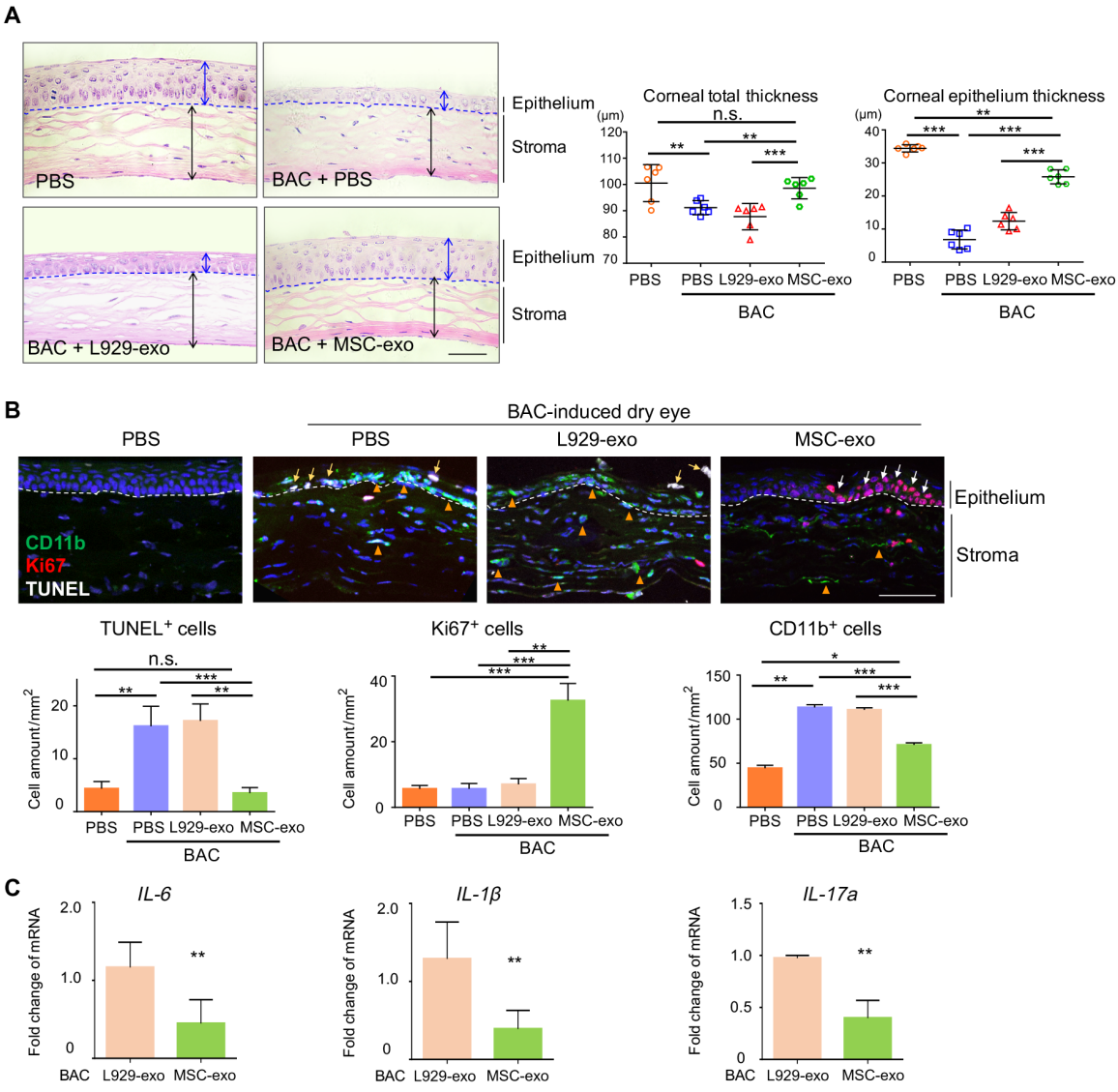

Fig. 4. MSC-exo could suppress the corneal inflammation during dry eye. (**A**) Corneal sections by hematoxylin and eosin staining revealed substantial loss of epithelium in the PBS and L929-exo treatment groups in BAC model, with reduced thicknesses of the total central cornea and the epithelium layer. After MSC-exo treatment, the BAC-stimulated cornea exhibited a regular and well-organized corneal structure, with corneal thickness recovery. $n = 6$ eyes, one-way ANOVA and Tukey's post hoc test. Scale bar, 50 μm. (**B**) Immunofluorescence of corneal section revealed decreased TUNEL$^+$ corneal cells, increased Ki-67$^+$ proliferative cells, and less CD11b$^+$ macrophage infiltration in the MSC-exo group in comparison to the PBS or L929-exo treatment group. $n = 3$ eyes, one-way ANOVA and Tukey's post hoc test. Scale bar, 50 μm. (**C**) In comparison to the L929-exo group, the MSC-exo group displayed reduced levels of proinflammatory cytokines, including *Il-6*, *Il-1*β, and *Il-17a*. $n = 6$ eyes, unpaired Student's *t* test. $^*P < 0.05$, $^{**}P < 0.01$, and $^{***}P < 0.001$.

BAC-induced dry eye mouse model. Consistent with the antixerophthalmic effect of miR-204, treatment of BAC-induced dry eye with either L929-miR-204-exo or MSC-exo markedly decreased the frequency of CD86$^+$ M1 macrophages, while it substantially increased CD206$^+$ M2 in the BAC-induced corneal whole mount (Fig. 7A) or on fluorescence-activated cell sorting (FACS) plots and graphs (Fig. 7B). Similarly, mRNA expression of M1-related genes was markedly reduced in L929-miR-204-exo and MSC-exo treatment groups (Fig. 7C). On the other hand, pretreatment with antagomiR-204 induced the increase of M1-related genes (fig. S7, A and B), indicating that miR-204 suppressed M1 gene expression program, and this might contribute to the alterations of M1 transcriptome.

To identify the downstream targets of miR-204, we undertook the bioinformatic approach using TargetScan 6.0, microRNA.org, and miRBase. The regulation network of the predicted targeted genes of miR-204 is shown in Fig. 7D, and we focused on *Il-6r*, which is highly expressed in macrophage and plays a critical role in its function (*38*). To address whether miR-204-5p plays a direct role on IL-6/IL-6R signaling, we performed luciferase reporter assay and confirmed a direct interaction of miR-204-5p with the 3′ untranslated region (3′UTR) of the *Il-6r* gene (Fig. 7E). We also show that miR-204 down-regulated IL-6 signaling correlated with the suppression of phospho-Stat3 (p-Stat3) activation and the expression of *Il-6* in Raw264.7 macrophages (Fig. 7F). Furthermore, small interfering RNA (siRNA)–mediated knockdown

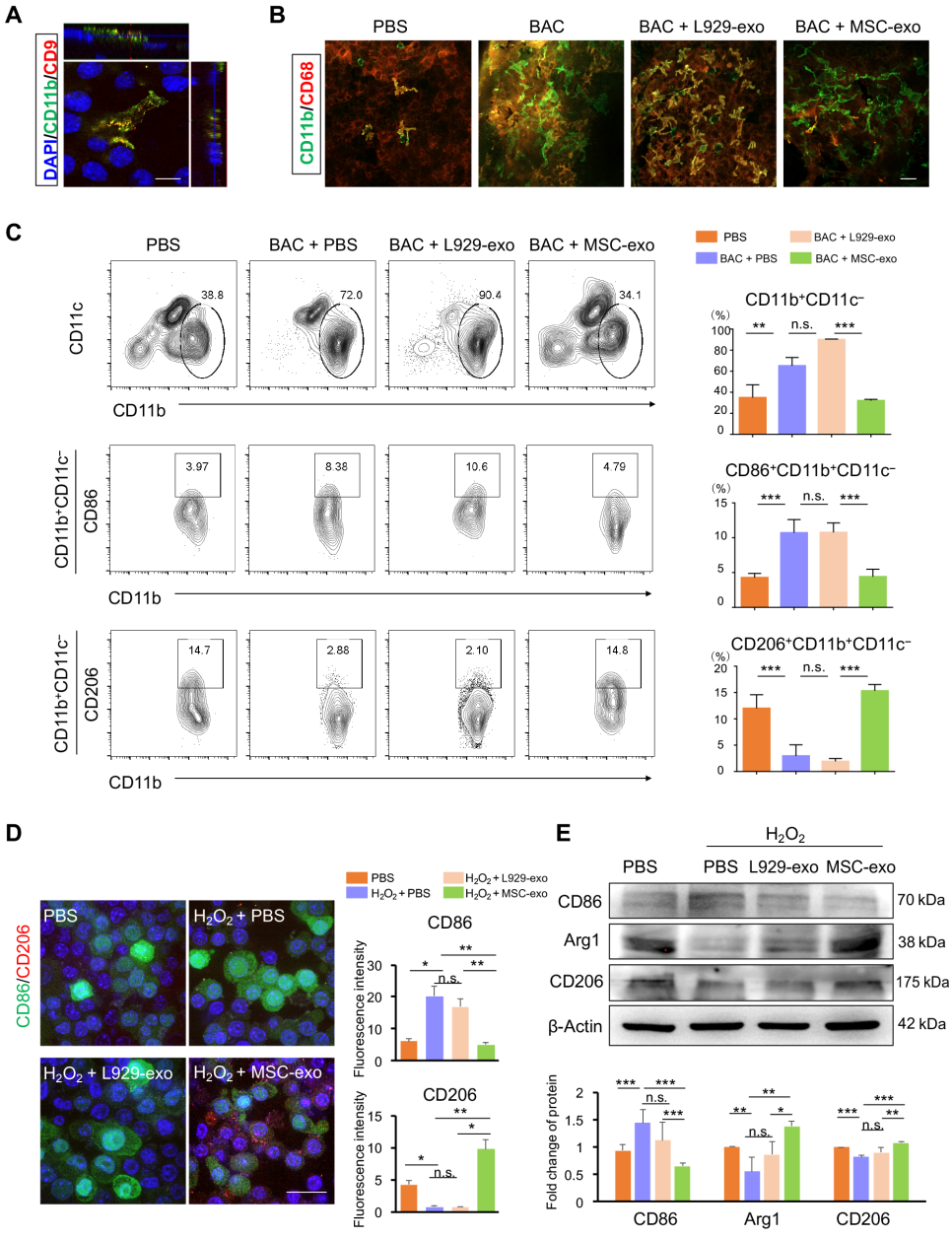

Fig. 5. Macrophages were reprogrammed by MSC-exo from M1 to M2 phenotype in vivo and in vitro. (**A**) $CD9^+$ exosomes were isolated from MSCs transfected with CD9-Tdtomato vector and administered as eye drops to BAC-stimulated mice. Immunochemical analysis of corneal whole mounts detected the colocalization of CD9-Tdtomato-MSC-exo with $CD11b^+$ macrophages, suggesting that macrophages were targets of MCS-exo in the cornea. Scale bar, 10 μm. (**B**) Detection of reduced numbers of $CD68^+CD11b^+$ activated macrophages in MSC-exo–treated corneal flat mounts. Scale bar, 50 μm. (**C**) Representative cytometry plots and graphs of $CD11b^+$ macrophages in the cornea of BAC-stimulated mice. Quadrants show percent CD11c-, CD86-, CD206-, and/or CD11b-expressing cells. $n = 12$ eyes (four corneas mixed in one sample), one-way ANOVA and Tukey's post hoc test. (**D**) The immunofluorescence of M1 and M2 marker (CD86 and CD206, respectively) on cultured raw264.7 macrophages. Scale bar, 50 μm. $n = 3$, one-way ANOVA and Tukey's post hoc test. (**E**) Western blot shows decreased expression of CD86, with increased Arg1 and CD206 expression after MSC-exo treatment in H_2O_2-stimulated raw264.7 cells. $n = 3$, one-way ANOVA and Tukey's post hoc test. $^*P < 0.05$, $^{**}P < 0.01$, and $^{***}P < 0.001$. DAPI, 4′,6-diamidino-2-phenylindole.

of IL-6 and IL-6R alleviates dry eye symptoms in mice, suggesting that the therapeutic effects of MSC-exo–miR-204 derive, at least in part, from targeted inhibition of IL-6/IL-6R axis (fig. S8, A and B). The increase of $CD206^+$ M2 macrophages induced by IL-6–siRNA and IL-6R–siRNA treatments also correlated with the reduction of M1-related gene expression (fig. S8, C and D). Together, our data suggest that miR-204/IL-6/IL-6R/Stat3 axis might regulate the macrophage differentiation program.

Last, as shown in a schematic diagram (Fig. 8), MSC-exo eye drop treatment is an efficient therapy for GVHD-associated dry eye disease via delivering its miR-204 cargo. The miR-204 in MSC-exo directly targeted *Il-6r* gene and suppressed the activation of IL-6R/Stat3 pathway,

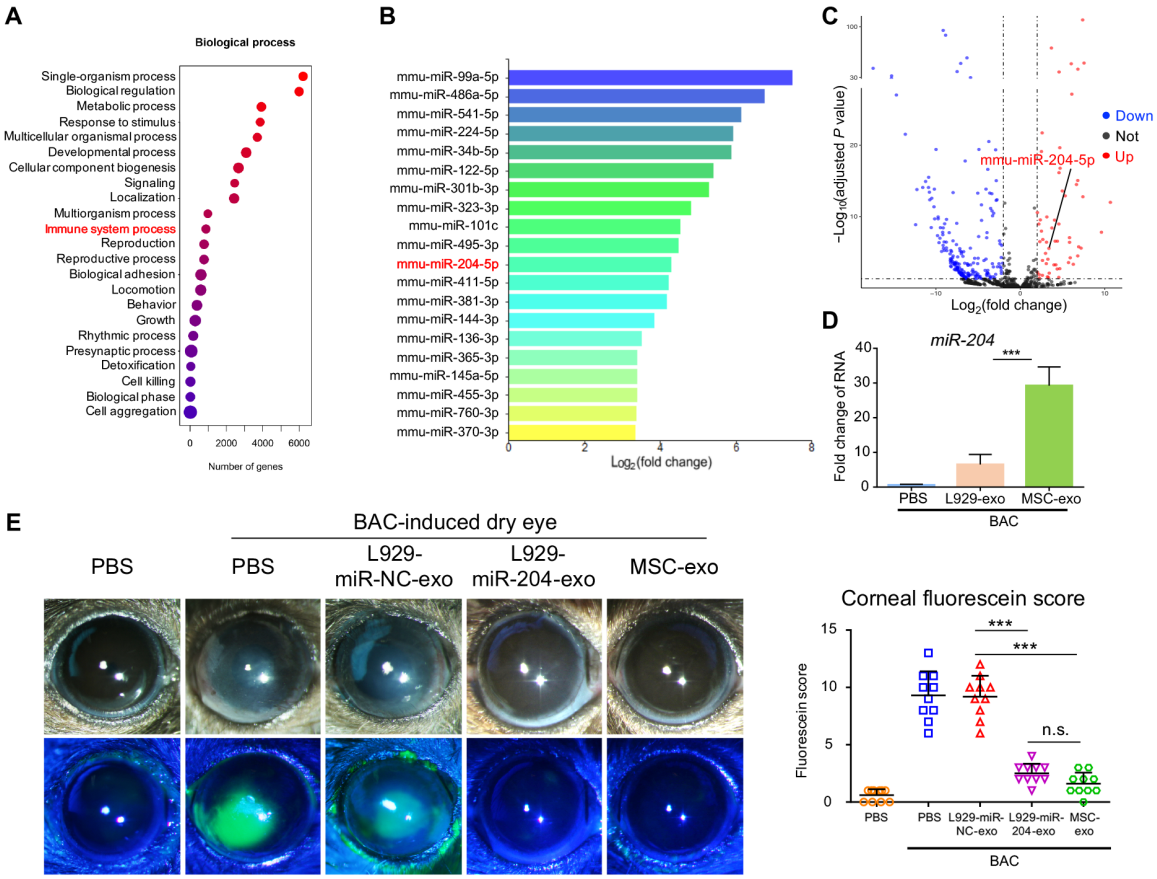

Fig. 6. miR-204 was required for the antixerophthalmic effect of MSC-exo. (**A**) miRNA profiling assays were performed on L929-exo and MSC-exo and GO analysis of the target genes of differentially expressed miRNAs in various processes. (**B**) Differentially up-regulated miRs in MSC-exo that target genes involved in the regulation of immune responses. (**C**) Volcano plot of differentially expressed miRNAs in MSC-exo than L929-exo. Red dots, up-regulated miRNAs; blue dots, down-regulated miRNAs with a >2.0-fold change. (**D**) qPCR analysis of miR-204-5p expression in the cornea tissue after MSC-exo treatment. $n = 6$ eyes, one-way ANOVA and Tukey's post hoc test. (**E**) Slit lamp and fluorescein staining analysis of BAC-stimulated mice treated with PBS or exosomes indicated in the figure. Fluorescein staining scores are indicated in the right. L929-miR-204-exo showed similar therapeutic potential with the MSC-exo group. $n = 10$ mice, one-way ANOVA and Tukey's post hoc test. ***$P < 0.001$.

reprogramming M1 macrophages to M2 and restoring the ocular surface homeostasis in the GVHD-associated dry eye disease.

DISCUSSION

GVHD-associated dry eye disease is devastating with limited therapeutic options as the patients usually fail to respond to current drugs, rendering them to suffer from unbearable pain and apparent visual impairment, severely affecting their quality of life (*39*). MSC-based cell therapies have been investigated for the treatment of multiple human autoimmune and inflammatory diseases including GVHD in the past decade (*40*). The exosomes secreted by MSCs were identified as the major executor to modulate the immune response, and their cell-free advantage facilitated them to be a promising alternative for MSC therapy (*41*). In a previous study, systemic treatment of MSCs by intravenous injection could improve the relief of dry eye symptoms in 12 of 22 patients with refractory GVHD (*42*). The relative stable property of exosomes and eye drops as a noninvasive way leads to applying exosome eye drops rather than MSC injection as therapeutic approaches. In this study, all the enrolled patients presented with improvements after MSC-exo eye drops, with relieved dry eye symptoms including sting, burn, crust, and redness. It is hard to compare their efficacy because of the difference in patients' inclusion criteria between these two studies. Actually, for the patients whose dry eye symptoms persist after the other target organ symptoms of chronic GVHD were relieved by systemic treatments, topical therapies such as MSC-exo may be an optimal option.

In the current trial, all the enrolled patients have used long-term artificial tears but presented no relief of dry eye symptoms. Some of them exhibit certain degree of responses to the steroid or nonsteroidal anti-inflammatory eye drops initially but develop resistance later. As we have known, artificial tears are usually administrated for complementing the insufficiency of tears but are unable to suppress the inflammatory injuries and prevent the progression of dry eye disease (*43*). By contrast, MSC-exo exert their therapeutic effects by suppressing the inflammatory injuries and maintaining the ocular surface homeostasis. In addition, the steroid and immunosuppressants are nonspecific and hardly restore the immune homeostasis in the ocular surface. Long-term steroid is always avoided in clinic because of an increased risk of side effects including infection, glaucoma, and cataract (*44*). In this study, when the symptoms were relieved after MSC-exo treatment, some patients reduced the use of the original

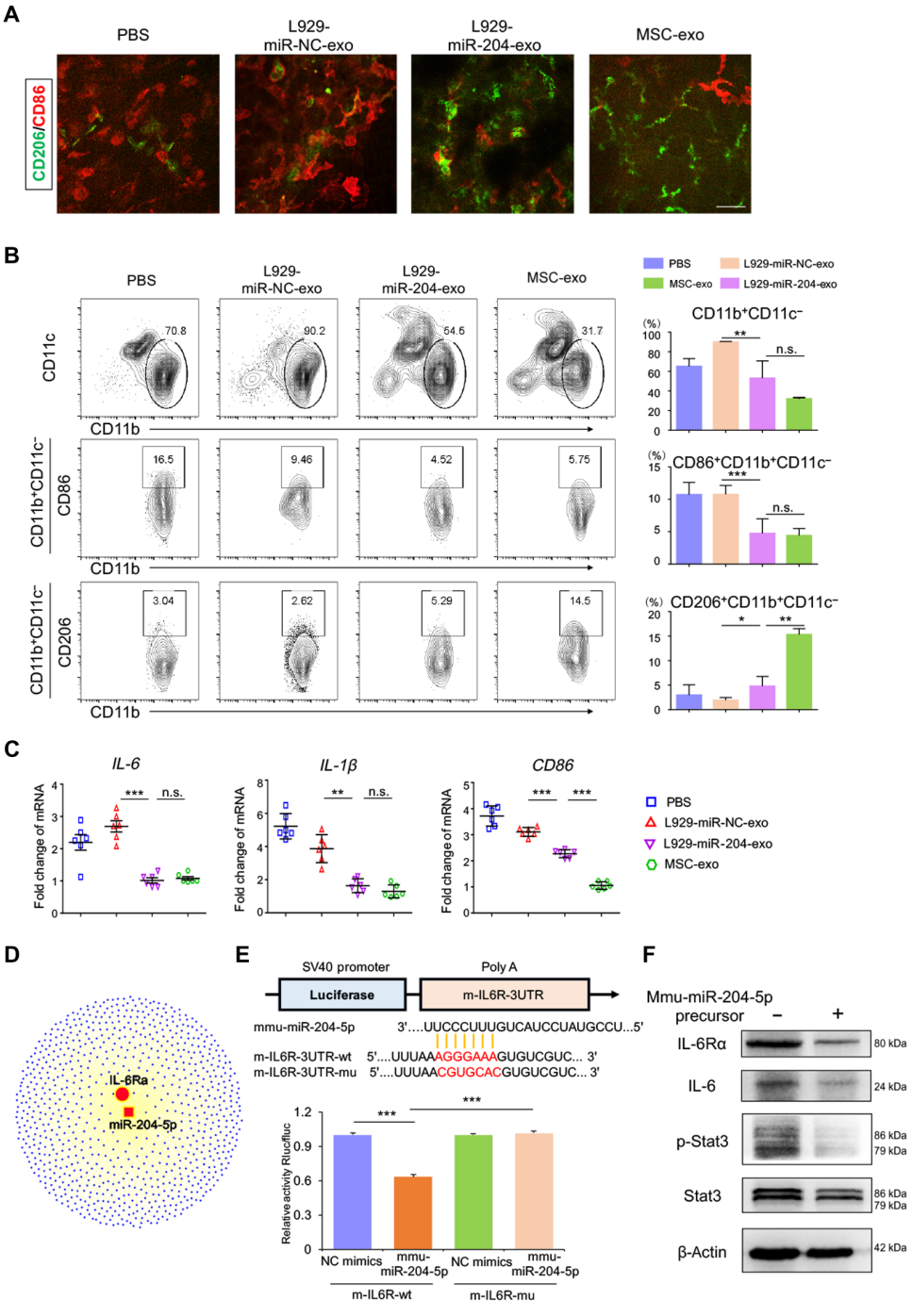

Fig. 7. miR-204 was the candidate mediator of MSC-exo for macrophage reprogramming from M1 to M2 by targeting IL-6R signaling. (**A**) L929-miR-204-exo and MSC-exo treatments suppressed the CD86$^+$ M1 macrophages and promoted CD206$^+$ M2 ones in the BAC-induced corneal whole-mount staining. Scale bar, 50 μm. (**B**) Flow cytometry showed that, in the BAC-induced dry eye corneas, the percentage of CD11b$^+$CD11c$^-$ macrophages decreased after L929-miR-204-exo or MSC-exo treatment compared with L929-miR-NC-exo controls, with more prominent reduction in the MSC-exo group. In addition, both treatments inhibited the percentage of CD11b$^+$CD11c$^-$CD86$^+$ M1 macrophages to a similar extent. $n = 12$ eyes (four corneas mixed in one sample), one-way ANOVA and Tukey's post hoc test. (**C**) mRNA expressions of IL-6, IL-1β, and CD86 were decreased after L929-miR-204-exo and MSC-exo treatments in comparison to the L929-miR-NC-exo group. $n = 6$ eyes, one-way ANOVA and Tukey's post hoc test. (**D**) Predicted regulatory networks of genes targeted by miR-204. (**E**) Luciferase reporter assay demonstrating direct interaction of miR-204-5p with 3′UTR of the *Il-6r* gene. One-way ANOVA and Tukey's post hoc test. $n = 3$. $^*P < 0.05$, $^{**}P < 0.01$, and $^{***}P < 0.001$. (**F**) Western blot analysis showing the suppression of IL-6Rα, IL-6, and p-Stat3 by mmu-miR-204-5p precursor.

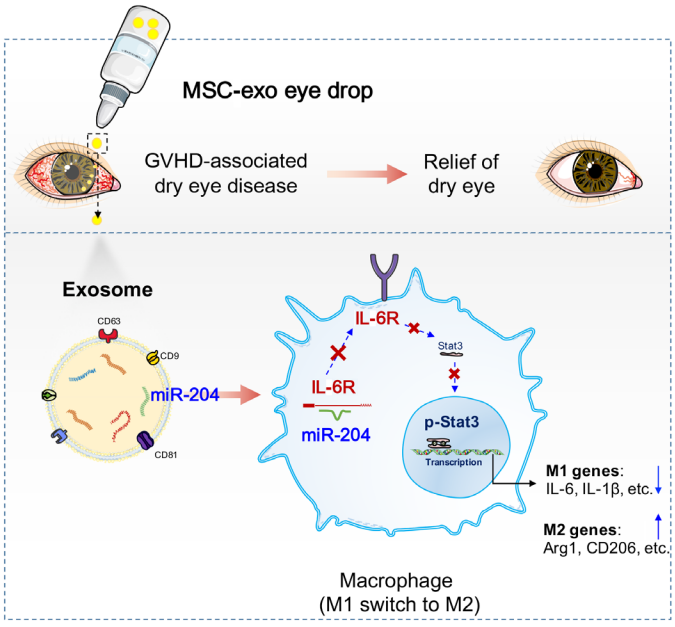

Fig. 8. Schematic drawing showing that MSC-exo eye drops alleviate GVHD-associated dry eye disease by reprogramming M1 macrophages to M2 via miR-204–mediated targeting of IL-6R/Stat3 pathway. The miR-204 in MSC-exo directly targeted the *Il-6r* gene and suppressed the activation of IL-6R/Stat3 pathway, resulting in the M1 macrophages in the dry eye cornea to reprogram toward immunosuppressive M2 phenotype. MSC-exo, which are enriched in miR-204, could restore the ocular surface homeostasis by switching M1 to M2 and ameliorate the inflammatory destruction during the GVHD-associated dry eye disease.

drugs, indicating that the MSC-exo treatment is a promising candidate. During the trial, some patients complained of transient irritation shortly after topical administration of MSC-exo eye drops. The patients have not reported any systemic complications relevant to MSC-exo treatment. Considering the immunoregulatory property of MSC-exo, long-term usage of MSC-exo may increase the risk of side effects similar to those of steroid or immunosuppressive drugs, such as infection, glaucoma, or cataract. The long-term efficacy and safety of MSC-exo eye drops are also important and needed to be evaluated in further investigation.

Although the pathogenesis of GVHD-associated dry eye disease remains unclear, researches consider it as a multifactorial disease characterized by a loss of immune homeostasis of the ocular surface (*45*). Infiltration of CD4 and CD8 T cells as well as other immune cells such as macrophages and mononuclear cells was also observed in the lacrimal gland, cornea, and conjunctiva in both mouse GVHD models (*2*, *5*) and human patients with mild or severe ocular GVHD (*7*–*9*). For example, Peszkowski *et al.* (*46*) showed that the rat GVHD model displayed markedly increased CD4 and CD8 T cells in the lacrimal glands at day 7 after the first perioral signs of GVHD. The conjunctiva-associated lymphoid tissue (CALT) and the closely related tear duct–associated lymphoid tissue with abnormal stimulation or structure were also believed to be crucial for the pathogenesis (*47*). Loss of epithelial integrity and potential presentation of antigens in CALT, which is composed of mainly effector lymphocytes and also innate effector cells, would lead to a loss of immune tolerance and the induction of inflammatory immune responses by, e.g., T helper 1 (T_H1) or T_H17 cells (*48*). The recruited T cells and other immune cells in the target ocular tissues were shown to express specific markers, such as CD154 on T cells or $CD86^+/CD40^+$ on macrophages, consistent with an activated phenotype (*11*). These activated macrophages displayed remarkable phenotypic plasticity and functional diversity due to their heterogeneous and phenotype shift. In general, M1 macrophages could produce proinflammatory cytokines [IL-1β, tumor necrosis factor–α (TNF-α), IL-6, etc.] and induce inflammation and tissue destruction. In contrast, the M2 macrophages are characterized by high expression of CD206 and Arg1 and production of an anti-inflammatory cytokine that resolves inflammation and promotes wound healing (*49*). As macrophage acts as a "double-edged sword" because of the M1 and M2 phenotypes, the indiscriminate inhibition of macrophage activation has failed to improve tissue regeneration and recovery. Instead, the modulation of macrophage polarization (M1/M2 shift) seems to be a promising therapeutic strategy for many inflammatory diseases (*50*). In this study, we found M1 macrophages ($CD86^+CD11b^+CD11c^-$) as the dominant macrophage subset that infiltrated the cornea during dry eye in the mouse model, and their levels substantially decreased following MSC-exo treatment. On the other hand, the proportion of anti-inflammatory M2 macrophages ($CD206^+CD11b^+CD11c^-$) was relatively low in mice with dry eye disease, but their numbers increased markedly following treatment with MSC-exo. Thus, activated M1 macrophages that infiltrated local ocular surface tissue may initiate the production of a cytokine storm that induces corneal pathological development of dry eye disease, while MSC-exo promote the M1 macrophages to reprogram into M2 phenotype and improve tissue recovery and homeostasis of the ocular surface. Together, our results suggested that MSC-exo not only suppressed the macrophage infiltration and activation in the eye but also modulated their phenotype shifts effectively.

MSC-exo carry a complex cargo of nucleic acids, proteins, and lipids, of which miRNAs have been recognized to be deeply implicated in intercellular communication (*51*). miRNA in exosomes could be efficiently integrated by specific recipient cells and regulate the cellular functions persistently (*52*). It is therefore important to note the miRNA content comparison analysis between MSC-exo and L929-exo. From the Gene Ontology (GO) analysis on the targeting genes of the differentially expressed miRNAs, we found that the immune system process was among the top-ranked biological processes, and then, we pulled out all the notably up-regulated miRNAs in MSC-exo whose target genes are involved in the regulation of immune responses. Among these miRNA candidates, the miR-204-5p is one of the most abundant miRNAs in MSC-exo. It is the most studied one, and its activity critically contributes to both ocular development and corneal repair (*34*–*36*). Furthermore, subconjunctival injection of BAC mice with antagomiR-204 abrogated the ability of MSC-exo to confer the protection from GVHD-associated dry eye disease, while L929-miR-204-exo eye drops ameliorated dry eye in mice. In addition, L929-miR-204-exo showed similar therapeutic effects as MSC-exo, indicating that MSC-exo mediated the therapeutic effects on dry eye disease through miR-204. Despite this, the cooperative regulation among multiple miRNAs would not be excluded for contributing to the effect of MSC-exo. Despite multiple targets of miR-204 that have been identified, we detected *Il-6r*, a predominant gene regulating macrophage functions, as the target of miR-204-5p. We went further to demonstrate that this particular interaction of miR-204 and IL-6R mediated the down-regulation of IL-6/IL-6R/Stat3 signaling, which is primarily responsible for macrophage phenotype

transition and alleviation of dry eye. siRNA-mediated knockdown of IL-6 and IL-6R alleviated dry eye symptoms, further suggesting that the therapeutic effects of MSC-exo-miR-204 might derive from targeted inhibition of IL-6/IL-6R axis. The evidence linked exosomal miR-204 to IL-6/IL-6R/Stat3 signaling, and hence, the suppression of M1 macrophages sheds new light on the MSC-exo therapeutic action.

Exosomes have been proved to be ideal cargos for drug delivery in comparison to other RNA-based therapy. Exosomes could avoid the challenges including instability, rapid degradation, and difficulties in delivering to target tissues in vivo. The advantages of exosomes make them attractive and potential for treating many diseases. The specific structure of phospholipid bilayer lets exosomes protect their contents from in vivo degradation (*53*). In contrast, the small RNA-based therapy still faces the challenge of instability and easy degradation. They have poor delivery and need to be packed with positively charged polymers to allow them to cross over the cell membrane, which may cause cytotoxicity. In addition, exosomes have some advantages over a small-molecular inhibitor of IL-6R. The reported small-molecular inhibitors of IL-6/IL-6R have a higher likelihood for off-target effects, since the binding region of IL-6–IL-6R–gp130 is too complex and broad, and are thus associated with adverse reactions (*54*). In contrast, exosomes are natural components of human body fluids and are generally considered safe, nontoxic, and less immunogenic (*55*). Here, topical eye drop usage of L929-miR-204-exo also presented a potential therapeutic effect similar to that of MSC-exo, indicating that engineering exosomes that integrated needed properties such as miR-204, which could be manufactured at large scale, are the future direction of development and facilitate miRNA-based therapy.

A major limitation of this prospective clinical trial, which has been approved to examine whether MSC-exo eye drop therapy would be effective in patients with GVHD-associated dry eye disease, is its relatively small sample size and short-term follow-up. In addition, MSC-exo therapy still faces the challenges for clinical applications, including the stability during storage and transport and the heterogeneity of exosome composition because of the culture conditions and purification methods (*20*, *56*). Mechanistically, our conclusion that MSC-exo treatment mediates its immuno-regulatory effects through miR-204 was, to a large extent, based on the demonstration that L929-miR-204-exo alleviated dry eye symptoms in two mouse models. Current mouse models could provide some mechanistic insights but still have certain limitations in mimicking the pathological development of GVHD-associated dry eye disease. Moreover, because of the complexity of the exosome content, we cannot exclude the roles of other elements such as mRNAs, noncoding RNAs, or proteins.

In summary, our findings demonstrated that MSC-exo exhibit a promising therapeutic effect on both mouse models of BAC induction and GVHD-associated dry eye disease. In particular, the antixerophthalmic efficacy of MSC-exo identified in our clinical study provided a possibility for extended application of MSC-exo in other severe dry eye diseases such as Sjogren's syndrome and other connective tissue diseases. It would be promising and interesting to enroll patients with wider spectrum of severe dry eye diseases for longer follow-up to get a more reliable conclusion. Mechanistically, MSC-exo could reprogram the M1 macrophages to anti-inflammatory M2, orchestrating the immune homeostasis in the ocular surface. miR-204 in exosomes is the mediator candidate by directly targeting on IL-6R and suppressing the activation of IL-6/IL-6R/Stat3 pathway to modulate macrophage phenotypes. Together, we posit that miR-204–containing MSC-exo eye drops can be exploited as a safe and noninvasive therapy for human dry eye disease and that miR-204/IL-6/Stat3 axis plays critical roles in maintaining ocular surface homeostasis and corneal transparency by regulating the balance between M1 and M2 macrophages on the ocular surface.

MATERIALS AND METHODS

Patient enrollment and examination

The patients diagnosed as chronic GVHD based on the National Institutes of Health (NIH) criteria and those complaining of dry eye symptoms were enrolled in this clinical trial (*39*). These patients presented with controlled and stable systematic GVHD signs on other organs but showed poor responses to the available ocular treatments, including artificial tears, glucocorticoid, immunosuppressor, or punctal occlusion. Thus, they were diagnosed with refractory GVHD–associated dry eye disease. Patients who met the inclusion and exclusion criteria were recruited in this trial (Supplementary Text). All patients signed the informed consents, and the baseline of clinical indicators including corneal fluorescein score, Schirmer's test, tear-film breakup time, and OSDI scores was recorded and scaled as previously described (*57*–*59*). Then, the enrolled eyes received 10 μg/50 μl of UC-MSC-exo eye drops four times a day for continuous 14 days. In the clinic, the patients who received eye drops were educated to press on the lacrimal duct area to minimize nasal mucosa or systemic absorption. The clinical indicators were monitored, and any side effects or adverse events relevant to topical application of the MSC-exo eye drops would be recorded during the follow-up. The clinical trial was conducted under the guidance of Good Clinical Practice standards and the Declaration of Helsinki, 1989, and the protocol was approved by the Ethics Committee of Zhongshan Ophthalmic Center, Sun-Yat Sen University (no. 2019KYPJ048) and registered at www.clinicaltrials.gov (NCT04213248).

MSC culture and exosome preparation

The exosomes used for clinical patients were derived from human UC-MSCs, and the exosomes used in vitro and in mice were derived from murine bone marrow MSCs. For human MSCs, the umbilical cords were rinsed twice with PBS supplemented with penicillin and streptomycin, and the cord vessels were removed. The washed cords were subsequently cut into small fragments that were individually attached to the substrate of culture plates and then were cultured in Dulbecco's modified Eagle's medium (DMEM) with 10% fetal bovine serum (FBS) and incubated at 37°C with 5% CO_2. The medium was replaced every 3 days after the initial culture, and well-developed colonies of fibroblast-like cells appeared about 10 days later. The colonies were then dissociated by 0.25% trypsin and further cultured. After three passages, cells were sorted by flow cytometry with negative markers of CD34-BV421 (562577, BD Pharmingen), CD45-PE (phycoerythrin) (304008, BioLegend), and CD11b-FITC (fluorescein isothiocyanate) (11-0118-42, eBioscience) and positive markers of CD44-FITC (11-0118-42, eBioscience), CD29-PE (12-0299-42, eBioscience), CD73-PerCP-Cy5.5 (561260, BD Pharmingen), CD166-BV421 (562936, BD Pharmingen), and CD105-APC (allophycocyanin) (562408, BD Pharmingen), and cells with multilineage differentiation ability were identified as human UC-MSCs, as previously described (*60*), which fulfill the minimal definition criteria proposed by the International Society for Cellular Therapy. The human UC-MSCs from passages 3 to 5 were used for the experiments.

Primary murine bone marrow MSCs were isolated and cultured as described previously (*61*). In brief, 4- to 6-week-old C57BL/6J mice were sacrificed by CO_2, and their tibia/fibula and femur were collected to extrude the bone marrow using a 22-gauge needle. The bone marrow cells were resuspended in DMEM/F-12 medium containing 10% FBS, penicillin (100 U/ml), and streptomycin (100 mg/ml) and seeded at a density of 1×10^6 cells/ml. The culture medium was changed 24 hours later and twice a week thereafter. The expanded cells were sorted by flow cytometry with negative markers of CD11b-FTIC (553310, BD Pharmingen), CD45-APC (559864, BD Pharmingen), and CD34-BV421 (562608, BD Pharmingen) and positive markers of CD44-PE (553134, BD Pharmingen), CD29-FITC (11-0291-82, eBioscience), and SCA-1-BV421 (108128, BioLegend). The cells were expanded in three to five passages for usage. The cell line of murine MSCs purchased from Cyagen Biosciences Inc. (MUBMX-01001) was also used. A CD9-TdTomato fusion protein expression vector (Mm01684; GeneCopoeia Inc., CA, USA) was used to transfect MSC line. After selection by puromycin-containing medium, MSCs stably expressing CD9-TdTomato were sorted by flow cytometry with TdTomato fluorescent. The murine fibroblast cell line L929 purchased from ScienCell Corporation (ScienCell Research Laboratories, Carlsbad, CA, USA) was used as the control of murine MSCs.

The exosome-free FBS used for MSC culture and supernatant collection was prepared by 100,000*g* centrifugation for 16 hours at 4°C with the deposits discarded. To manufacture exosomes, we chose the classical isolation method by ultracentrifugation to obtain exosome from supernatant of large volume, which is still considered as the "gold standard" for exosome isolation that minimally affects the membrane structure and contents (*62*). The cells were cultured in medium containing 10% exosome-free FBS for 48 hours, and culture supernatant was collected. Then, these supernatants were obtained by sequential centrifugation at 200*g* for 10 min, 2000*g* for 20 min, 10,000*g* for 30 min, and 100,000*g* for 2 hours at 4°C. The pellet was washed twice with PBS and filtered through the 0.22-μm filter. The prepared exosomes were stored until use at −80°C. The morphology and size distribution of exosomes were identified by transmission electron microscopy (FEI Tecnai 12, Philips, The Netherlands) and NanoSight tracking analysis (NanoSight NS300, Malvern, UK) as previously described (*63*). Markers of exosomes—including CD63, CD9, CD81, annexin A1, and HSP90—were analyzed by Western blot (*20*).

Mice and dry eye models

The C57BL/6J mice (6 to 8 weeks old; male versus female mice is 1:1) and male NCG mice were used for establishing dry eye models. NCG mice were purchased from the National Resource Center of Model Mice and Model Animal Research Center of Nanjing University. These mice were kept in a specific pathogen–free facility in the Animal Laboratories of Zhongshan Ophthalmic Center. This study was approved by the Ethics Committee of Zhongshan Ophthalmic Center, Sun-Yat Sen University (no. 2018-066). All the experiments were carried out in accordance with the approved guidelines of the Animal Care and Use Committee of Zhongshan Ophthalmic Center and the Association Research in Vision and Ophthalmology Statement for the Use of Animals in Ophthalmic and Vision Research.

BAC mice model was induced by 5-μl eye drops of 0.2% BAC (Sigma-Aldrich, St. Louis, MO, USA) twice a day for 7 days on C57BL/6J mice. These mice were randomly assigned to different treatment groups with 5 μl of eye drop per eye, twice a day for 7 days (MSC-exo in 0.5×10^{10}, 2.5×10^{10}, or 12.5×10^{10} particles/ml; L929-exo; artificial tears; PBS; L929-NC-miR-exo; or L929-miR-204-exo, respectively). The MSC-exo were preservative-free and had physiological osmolarity and pH comparable to those of the artificial tears. For the antagomiR treatment experiment, the MSC-exo–treated BAC mice simultaneously received 1 μl of 200 nM antagomiR-204 or antagomir-NC by subconjunctival injection on days 0, 3, and 6. For the experiment using IL-6/IL-6R siRNA treatment, the BAC mice were treated by subconjunctival injection of 1 μl of 50 μM IL-6-siRNA or IL-6R-siRNA on days 0, 3, and 6 for three times.

The NCG mice received 1×10^7 cells per 300 μl of human PBMCs by tail vein injection to establish GVHD model. Systematic symptoms including body weight loss, diarrhea, hair loss, and activities were monitored, and clinical scores were evaluated every 3 days as previously described (*64*). The histological analysis of typical organs is shown in fig. S9. When the mice could be diagnosed as GVHD and present classic dry eye symptoms including corneal defects, limbus palpebralis edema, and so on, they would receive respective treatments (2.5×10^{10}particles/ml, 5 μl per eye, twice a day for 7 days). The ocular surface examination was then performed.

Murine ocular surface examination

After anesthetizing by intraperitoneal injection of pentobarbital (0.05 mg/g body weight), tear quantity was measured using the cotton thread test (Zone-Quick, Showa Yakuhin Kako, Tokyo, Japan) without topical anesthetic. The thread was held with jeweler forceps and applied to the lateral canthus for 30 s and then turned red in contact with tears. Wetting of the thread was measured in millimeters under a dissecting microscope. Fluorescein staining was performed with 5 μl of 0.5% fluorescein sodium solution instilled into the conjunctival sac, and the mouse ocular surface was observed under a slit lamp microscope (Slit Lamp BX900; Haag-Streit, USA). The corneal epithelial damage was evaluated under a cobalt blue filter and divided into five parts, graded from 0 to 3 in each part (*65*).

Mmu-miR-204-5p precursor transfection of L929 and Raw264.7 cell

Fibroblast cell line L929 cells and macrophage cell line Raw264.7 were purchased from ScienCell Corporation (ScienCell Research Laboratories, Carlsbad, CA, USA). These cells were transfected with mmu-miR-204-5p precursor (HH20180611DZQ-LV01, Hanbio Biotechnology Co., Shanghai, China). Plasmid transfection was performed using Lipofectamine 2000 (Invitrogen) following the manufacturer's instructions. For the stable transfection of miRNAs, the cells were selected with puromycin (500 μg/ml; LOUNBIOTECH, Guangzhou, China) and sorted by a FACSAria I cell sorter (Becton-Dickinson, Franklin Lakes, NJ, USA). The sorted cells were cultured for expansion. The transfected L929 cells were cultured with exosome-free FBS, and the supernatants were collected to obtain exosomes by centrifugation. The Raw264.7 cells were pretreated with L929-exo or MSC-exo (2.5×10^5/ml, dissolved in PBS) for 2 hours and then stimulated with hydrogen peroxide (200 μM) or hypoxia (1% O_2, 5% CO_2, and balanced N_2) at 37°C for 24 hours, and then cells were harvested to analyze macrophage polarization states or miR-204–related signaling pathway activation.

Immunofluorescence staining

The cornea flat mounts, cryosections, and cultured cells were fixed in 4% paraformaldehyde and blocked with 0.5% Triton X-100/5% bovine serum albumin for 2 hours at room temperature. The samples were incubated with primary antibodies overnight at 4°C and

then with secondary antibodies for 1 hour. The primary antibodies included anti-CD11b antibody (ab8878, Abcam), anti-CD68 antibody (ab53444, Abcam), anti-CD86 antibody (ab119857, Abcam), anti-CD206 antibody (AF2535, R&D Systems), and anti-Ki67 antibody (ab16667, Abcam). Secondary antibodies included donkey anti-rabbit immunoglobulin G (IgG) (H + L) Alexa Fluor 555, donkey anti-rat IgG (H + L) Alexa Fluor 488, donkey anti-rabbit IgG (H + L) Alexa Fluor 488, and donkey anti-goat IgG (H + L) Alexa Fluor 555 secondary antibodies (1:1000; Invitrogen). TUNEL staining (In Situ Cell Death Detection Kit, Fluorescein; Roche, IN, USA) was performed according to the manufacturer's instructions. The corneal whole mounts were dissected into four petals and detected by ZEISS (LSM880, Germany). Three images of each petal were captured in mid-periphery areas of each cornea, respectively.

Hematoxylin and eosin staining

Eyes were fixed in formalin overnight, embedded in paraffin, and cut into 3-μm vertical slices. Sections were washed in deionized water for 5 min and incubated with hematoxylin buffer for 10 min at room temperature. Then, these sections were rinsed in deionized water and dipped in 1% eosin solution for 15 s. After rehydrating in alcohol gradients, slices were washed again and mounted. Histological analyses of corneal tissues were observed under a microscope (Leica DM4000, Germany), and images were processed and analyzed with ImageJ software (Public Domain, imagej.nih.gov/ij/). The thickness of the total cornea and corneal epithelium layer was counted and analyzed blindly by trained pathologists.

Flow cytometry

The corneas were dissected out and placed in 1 ml of RPMI with deoxyribonuclease I (0.002 g) and collagenase D (0.004 g) in a 37°C bath for 60 min, with inverting every 10 min while pipetting up and down. The digestion was stopped by 200 μl of FBS, and cell suspension was filtered through a 70-μm strainer (BD Biosciences, San Diego, CA, USA). The cells were washed with PBS containing 1% FBS and 1% Hepes (MP Biomedicals) and stained with CD45-APC (559864, BD Pharmingen), CD11b-BV421 (101236, BioLegend), CD11c-PerCP-Cy5.5 (45-0114-83, eBioscience), CD86-PE (553629, BD Pharmingen), and CD206-FITC (141704, BioLegend) antibodies for 30 min at room temperature. A multilaser Becton-Dickinson FACSCalibur (BD Biosciences) was used to collect the data, and FlowJo software was used for analysis.

Western blotting

The protein concentration was determined by bicinchoninic acid protein assay. Equal amount of protein was used, and Western blotting was performed as previously described (*66*). Primary antibodies included anti-CD9 antibody (ab92726, Abcam, MA), anti-CD63 antibody (216130, Abcam, MA), anti-CD81 antibody [10037, Cell Signaling Technology (CST)], anti–annexin A1 antibody (3299, CST), anti-HSP90 antibody (4877, CST), anti–IL-6R antibody (ab83053, Abcam, MA), anti-Stat3 antibody and anti-p-Stat3 antibody (9139S and 9145S, CST), anti–IL-6 antibody (12912, CST), anti–nuclear factor κB antibody (8242S, CST), anti–TNF-α antibody (ab1793, Abcam, MA), anti–IL-1b antibody (NB600-633, Novus), anti-CD86 antibody (ab119857, Abcam, MA), anti-Arg1 antibody (sc-18355, Santa Cruz Biotechnology, CA), and anti–β-actin antibody (ab28696, Abcam, MA). The gray intensity of protein blots was measured using ImageJ software (NIH).

Real-time PCR

The total RNA was extracted with TRIzol (Invitrogen, Carlsbad, CA, USA) and was converted into first-strand complementary DNA using the PrimeScript RT reagent Kit (TaKaRa Biotechnology Co. Ltd., Dalian, China) or riboSCRIPT Reverse Transcription Kit (RiboBio Co. Ltd., Guangzhou, China) according to the manufacturer's instructions. Quantitative real-time PCR experiments were performed with SYBR Green I in a LightCycler 96 (Roche Applied Science, Mannheim, Germany). The primers are listed in table S1. For normalization and relative quantification, *Gapdh* gene and U6 were used as reference genes. Expression was calculated by relative quantification using the $2-\Delta\Delta CT$ method.

Luciferase activity assay

Luciferase activity assays were conducted as reported previously (*67*). The wild-type IL-6R 3′UTR firefly luciferase reporter plasmids and IL-6R 3′UTR firefly luciferase reporter plasmids with the potential miR-204-5p binding site mutated were cotransfected with miR-204-5p mimics or miR-NC mimics to human embryonic kidney 293 cells, respectively. Renilla luciferase reporter plasmids were also transfected as internal control. The luciferase activities were measured by a Dual-Glo Luciferase Assay Kit (Promega) 48 hours after transfections.

RNA library construction and miRNA sequencing

For total RNA extraction from L929-exo and MSC-exo, TRIzol reagent (Invitrogen, Carlsbad, CA, USA) was used according to the manufacturer's instruction. Three experimental replicates per group were performed. The concentration and integrity of each RNA sample were measured by Agilent 2100 Bioanalyzer (Thermo Fisher Scientific, Waltham, MA, USA) and are shown in fig. S10. Library preparation and miRNA sequencing were performed by Biomarker Cloud Technologies Co. Ltd. (Beijing, China) using the miRNA library preparation kit. Standard polyacrylamide gel electrophoresis gel electrophoresis was used to examine RNA integrity. The clustering of the index-coded samples was performed on a cBot Cluster Generation System using the TruSeq PE Cluster Kit v4-cBot-HS (Illumia) according to the manufacturer's instructions. After cluster generation, the library preparations were sequenced on an Illumina platform, and single-end reads were generated. Raw reads of fastq format were first processed through in-house perl scripts followed by removing reads containing adapter, ploy-N, and low-quality reads. In addition, clean data were obtained by removing the sequences smaller than 15 nucleotides (nt) or longer than 35 nt. At the same time, Q20, Q30, GC content, and sequence duplication level of the clean data were calculated to ensure data with high quality.

Bioinformatic analysis

The reads were used to detect known miRNA and novel miRNA predicted by comparing with Genome and known miRNAs from miRBase. miRNA expression levels were estimated for each sample by mapping back onto the precursor sequence and obtaining read count for each miRNA from the mapping results. Differential expression analysis was performed using the DESeq2 R package (1.10.1). The resulting *P* values were adjusted using Benjamini and Hochberg's approach for controlling the false discovery rate (FDR). miRNAs with $|\log_2(FC)| \geq 1$; FDR ≤ 0.05 found by DESeq2 were assigned as differentially expressed. GO enrichment analysis of the differentially expressed genes was implemented by the GOseq R packages based on the Wallenius

noncentral hypergeometric distribution. All genes in GO term "immune system process" (0002376) were mapped to the annotated miR dataset with paired miR filtered. All miRs and immune-related miRs were ranged on the basis of the level of $\log_2$ fold change and were represented by bar chart and volcano plots drawn with ggplot2 v3.3.2. The RNA sequencing dataset was deposited in Gene Expression Omnibus (GSE166585). In addition, the target genes of mmu-miR-204-5p were illustrated by miRnet, a miRNA-centric network visual analytics platform, with 860 target genes based on the database TarBase v8.0.

Statistics

All experiments were performed at least two times, and biological replicates are indicated in the figure legends by *n*. The statistical analysis was performed using GraphPad Prism (GraphPad Software, version 6.0, La Jolla, USA). The differences of ocular examination results between D0 and D14 were analyzed using a paired Student's *t* test. All quantitative data are presented as means ± SEM, with the number of samples provided in the figure legends, which were analyzed by a two-tailed unpaired Student's *t* test (two groups) or one-way analysis of variance (ANOVA) (>2 groups) with Tukey's post hoc comparisons test. $P \leq 0.05$ was considered as statistically significant.

SUPPLEMENTARY MATERIALS

Supplementary material for this article is available at https://science.org/doi/10.1126/sciadv.abj9617

View/request a protocol for this paper from *Bio-protocol*.

REFERENCES AND NOTES

1. J. A. Clayton, Dry eye. *N. Engl. J. Med.* **378**, 2212–2223 (2018).
2. S. Herretes, D. B. Ross, S. Duffort, H. Barreras, T. Yaohong, A. M. Saeed, J. C. Murillo, K. V. Komanduri, R. B. Levy, V. L. Perez, Recruitment of donor T cells to the eyes during ocular GVHD in recipients of MHC-matched allogeneic hematopoietic stem cell transplants. *Invest. Ophthalmol. Vis. Sci.* **56**, 2348–2357 (2015).
3. G. Giannaccare, M. Pellegrini, F. Bernabei, V. Scorcia, E. Campos, Ocular surface system alterations in ocular graft-versus-host disease: All the pieces of the complex puzzle. *Graefes Arch. Clin. Exp. Ophthalmol.* **257**, 1341–1351 (2019).
4. D. J. Royer, J. Echegaray-Mendez, L. Lin, G. B. Gmyrek, R. Mathew, D. R. Saban, V. L. Perez, D. J. Carr, Complement and $CD4^+$ T cells drive context-specific corneal sensory neuropathy. *eLife* **8**, e48378 (2019).
5. A. S. Hassan, S. G. Clouthier, J. L. M. Ferrara, A. Stepan, S. I. Mian, A. Z. Ahmad, V. M. Elner, Lacrimal gland involvement in graft-versus-host disease: A murine model. *Invest. Ophthalmol. Vis. Sci.* **46**, 2692–2697 (2005).
6. Y. Maeda, P. Reddy, K. P. Lowler, C. Liu, D. K. Bishop, J. L. M. Ferrara, Critical role of host γδ T cells in experimental acute graft-versus-host disease. *Blood* **106**, 749–755 (2005).
7. M. Uchino, Y. Ogawa, M. Kawai, H. Shimada, K. Kameyama, S. Okamoto, M. Dogru, K. Tsubota, Ocular complications in a child with acute graft-versus-host disease following cord blood stem cell transplantation: Therapeutic challenges. *Acta Ophthalmol. Scand.* **84**, 545–548 (2006).
8. A. Kheirkhah, Y. Qazi, M. A. Arnoldner, K. Suri, R. Dana, In vivo confocal microscopy in dry eye disease associated with chronic graft-versus-host disease. *Invest. Ophthalmol. Vis. Sci.* **57**, 4686–4691 (2016).
9. A. Kheirkhah, R. Rahimi Darabad, A. Cruzat, A. R. Hajrasouliha, D. Witkin, N. Wong, R. Dana, P. Hamrah, Corneal epithelial immune dendritic cell alterations in subtypes of dry eye disease: A pilot in vivo confocal microscopic study. *Invest. Ophthalmol. Vis. Sci.* **56**, 7179–7185 (2015).
10. B. Rojas, R. Cuhna, P. Zafirakis, J. M. Ramirez, M. Lizan-garciía, T. Zhao, C. S. Foster, Cell populations and adhesion molecules expression in conjunctiva before and after bone marrow transplantation. *Exp. Eye Res.* **81**, 313–325 (2005).
11. Y. Ogawa, M. Kuwana, K. Yamazaki, Y. Mashima, M. Yamada, T. Mori, S. Okamoto, Y. Oguchi, Y. Kawakami, Periductal area as the primary site for T-cell activation in lacrimal gland chronic graft-versus-host disease. *Invest. Ophthalmol. Vis. Sci.* **44**, 1888–1896 (2003).
12. S. Sinha, R. B. Singh, T. H. Dohlman, M. Wang, Y. Taketani, J. Yin, R. Dana, Prevalence of persistent corneal epithelial defects in chronic ocular graft-versus-host disease. *Am. J. Ophthalmol.* **218**, 296–303 (2020).
13. Y. Ogawa, H. Kodama, K. Kameyama, K. Yamazaki, H. Yasuoka, S. Okamoto, H. Inoko, Y. Kawakami, M. Kuwana, Donor fibroblast chimerism in the pathogenic fibrotic lesion of human chronic graft-versus-host disease. *Invest. Ophthalmol. Vis. Sci.* **46**, 4519–4527 (2005).
14. A. Janin, T. Facon, P. Castier, E. Mancel, J. P. Jouet, B. Gosselin, Pseudomembranous conjunctivitis following bone marrow transplantation: Immunopathological and ultrastructural study of one case. *Hum. Pathol.* **27**, 307–309 (1996).
15. M. Pellegrini, F. Bernabei, F. Barbato, M. Arpinati, G. Giannaccare, P. Versura, F. Bonifazi, Incidence, risk factors and complications of ocular graft-versus-host disease following hematopoietic stem cell transplantation. *Am. J. Ophthalmol.* **227**, 25–34 (2021).
16. M. Balaram, S. Rashid, R. Dana, Chronic ocular surface disease after allogeneic bone marrow transplantation. *Ocul. Surf.* **3**, 203–210 (2005).
17. Y. Shi, Y. Wang, Q. Li, K. Liu, J. Hou, C. Shao, Y. Wang, Immunoregulatory mechanisms of mesenchymal stem and stromal cells in inflammatory diseases. *Nat. Rev. Nephrol.* **14**, 493–507 (2018).
18. N. Song, M. Scholtemeijer, K. Shah, Mesenchymal stem cell immunomodulation: Mechanisms and therapeutic potential. *Trends Pharmacol. Sci.* **41**, 653–664 (2020).
19. C. Thery, L. Zitvogel, S. Amigorena, Exosomes: Composition, biogenesis and function. *Nat. Rev. Immunol.* **2**, 569–579 (2002).
20. D. K. Jeppesen, A. M. Fenix, J. L. Franklin, J. N. Higginbotham, Q. Zhang, L. J. Zimmerman, D. C. Liebler, J. Ping, Q. Liu, R. Evans, W. H. Fissell, J. G. Patton, L. H. Rome, D. T. Burnette, R. J. Coffey, Reassessment of exosome composition. *Cell* **177**, 428–445.e18 (2019).
21. A. Casado-Diaz, J. M. Quesada-Gomez, G. Dorado, Extracellular vesicles derived from mesenchymal stem cells (MSC) in regenerative medicine: Applications in skin wound healing. *Front. Bioeng. Biotechnol.* **8**, 146 (2020).
22. T. R. Doeppner, M. Bähr, D. M. Hermann, B. Giebel, Concise review: Extracellular vesicles overcoming limitations of cell therapies in ischemic stroke. *Stem Cells Transl. Med.* **6**, 2044–2052 (2017).
23. R. Kalluri, V. S. LeBleu, The biology, function, and biomedical applications of exosomes. *Science* **367**, eaau6977 (2020).
24. W. Ouyang, Y. Wu, X. Lin, S. Wang, Y. Yang, L. Tang, Z. Liu, J. Wu, C. Huang, Y. Zhou, X. Zhang, J. Hu, Z. Liu, Role of $CD4^+$ T helper cells in the development of BAC-induced dry eye syndrome in mice. *Invest. Ophthalmol. Vis. Sci.* **62**, 25 (2021).
25. Z. Lin, X. Liu, T. Zhou, Y. Wang, L. Bai, H. He, Z. Liu, A mouse dry eye model induced by topical administration of benzalkonium chloride. *Mol. Vis.* **17**, 257–264 (2011).
26. R. Samaeekia, B. Rabiee, I. Putra, X. Shen, Y. J. Park, P. Hematti, M. Eslani, A. R. Djalilian, Effect of human corneal mesenchymal stromal cell-derived exosomes on corneal epithelial wound healing. *Invest. Ophthalmol. Vis. Sci.* **59**, 5194–5200 (2018).
27. L. Yin, X. J. Wang, D. X. Chen, X. N. Liu, X. J. Wang, Humanized mouse model: A review on preclinical applications for cancer immunotherapy. *Am. J. Cancer Res.* **10**, 4568–4584 (2020).
28. X. Wu, Y. Li, B. Huang, X. Ma, L. Zhu, N. Zheng, S. Xu, W. Nawaz, C. Xu, Z. Wu, A single-domain antibody inhibits SFTSV and mitigates virus-induced pathogenesis in vivo. *JCI Insight* **5**, e136855 (2020).
29. D. Zhou, Y. T. Chen, F. Chen, M. Gallup, T. Vijmasi, A. F. Bahrami, L. B. Noble, N. van Rooijen, N. A. McNamara, Critical involvement of macrophage infiltration in the development of Sjögren's syndrome-associated dry eye. *Am. J. Pathol.* **181**, 753–760 (2012).
30. I. C. You, T. G. Coursey, F. Bian, F. L. Barbosa, C. S. de Paiva, S. C. Pflugfelder, Macrophage phenotype in the ocular surface of experimental murine dry eye disease. *Arch. Immunol. Ther. Exp. (Warsz.)* **63**, 299–304 (2015).
31. J. Pajarinen, T. Lin, E. Gibon, Y. Kohno, M. Maruyama, K. Nathan, L. Lu, Z. Yao, S. B. Goodman, Mesenchymal stem cell-macrophage crosstalk and bone healing. *Biomaterials* **196**, 80–89 (2019).
32. H. S. Lee, J.-H. Choi, L. Cui, Y. Li, J. M. Yang, J.-J. Yun, J. E. Jung, W. Choi, K. C. Yoon, Anti-inflammatory and antioxidative effects of *Camellia japonica* on human corneal epithelial cells and experimental dry eye: In vivo and in vitro study. *Invest. Ophthalmol. Vis. Sci.* **58**, 1196–1207 (2017).
33. A. Robson, Exosome-derived microRNAs improve cardiac function. *Nat. Rev. Cardiol.* **18**, 150–151 (2021).
34. L. Latta, N. Ludwig, L. Krammes, T. Stachon, F. N. Fries, A. Mukwaya, N. Szentmary, B. Seitz, B. Wowra, M. Kahraman, A. Keller, E. Meese, N. Lagali, B. Kasmann-Kellner, Abnormal neovascular and proliferative conjunctival phenotype in limbal stem cell deficiency is associated with altered microRNA and gene expression modulated by PAX6 mutational status in congenital aniridia. *Ocul. Surf.* **19**, 115–127 (2021).
35. A. Shiels, TRPM3_miR-204: A complex locus for eye development and disease. *Hum. Genomics* **14**, 7 (2020).
36. Y. Lu, P. W. L. Tai, J. Ai, D. J. Gessler, Q. Su, X. Yao, Q. Zheng, P. D. Zamore, X. Xu, G. Gao, Transcriptome profiling of neovascularized corneas reveals miR-204 as a multi-target biotherapy deliverable by rAAVs. *Mol. Ther. Nucleic Acids* **10**, 349–360 (2018).

37. T. Li, H. Pan, R. Li, The dual regulatory role of miR-204 in cancer. *Tumour Biol.* **37**, 11667–11677 (2016).
38. S. Tajima, K. Tsuji, Y. Ebihara, X. Sui, R. Tanaka, K. Muraoka, M. Yoshida, K. Yamada, K. Yasukawa, T. Taga, T. Kishimoto, T. Nakahata, Analysis of interleukin 6 receptor and gp130 expressions and proliferative capability of human CD34+ cells. *J. Exp. Med.* **184**, 1357–1364 (1996).
39. R. Jacobs, U. Tran, H. Chen, A. Kassim, B. G. Engelhardt, J. P. Greer, S. G. Goodman, C. Clifton, C. Lucid, L. A. Vaughan, B. N. Savani, M. Jagasia, Prevalence and risk factors associated with development of ocular GVHD defined by NIH consensus criteria. *Bone Marrow Transplant.* **47**, 1470–1473 (2012).
40. O. Levy, R. Kuai, E. M. J. Siren, D. Bhere, Y. Milton, N. Nissar, M. De Biasio, M. Heinelt, B. Reeve, R. Abdi, M. Alturki, M. Fallatah, A. Almalik, A. H. Alhasan, K. Shah, J. M. Karp, Shattering barriers toward clinically meaningful MSC therapies. *Sci. Adv.* **6**, eaba6884 (2020).
41. K. Yin, S. Wang, R. C. Zhao, Exosomes from mesenchymal stem/stromal cells: A new therapeutic paradigm. *Biomark. Res.* **7**, 8 (2019).
42. J. Weng, C. He, P. Lai, C. Luo, R. Guo, S. Wu, S. Geng, A. Xiangpeng, X. Liu, X. Du, Mesenchymal stromal cells treatment attenuates dry eye in patients with chronic graft-versus-host disease. *Mol. Ther.* **20**, 2347–2354 (2012).
43. L. Jones, L. E. Downie, D. Korb, J. M. Benitez-Del-Castillo, R. Dana, S. X. Deng, P. N. Dong, G. Geerling, R. Y. Hida, Y. Liu, K. Y. Seo, J. Tauber, T. H. Wakamatsu, J. Xu, J. S. Wolffsohn, J. P. Craig, TFOS DEWS II management and therapy report. *Ocul. Surf.* **15**, 575–628 (2017).
44. P. S. Severn, S. G. Fraser, Bilateral cataracts and glaucoma induced by long-term use of oral prednisolone bought over the internet. *Lancet* **368**, 618 (2006).
45. S. Z. Munir, J. Aylward, A review of ocular graft-versus-host disease. *Optom. Vis. Sci.* **94**, 545–555 (2017).
46. M. J. Peszkowski, K. Fujiwara, G. Warfvinge, A. Larsson, Experimental graft versus host disease in the (BN × LEW) F1 rat hybrid as a model for autoimmune disease. Study of early adenitis in lacrimal and salivary glands. *Autoimmunity* **24**, 101–111 (1996).
47. R. Mastropasqua, L. Agnifili, V. Fasanella, M. Nubile, A. A. Gnama, G. Falconio, P. Perri, S. Di Staso, C. Mariotti, The conjunctiva-associated lymphoid tissue in chronic ocular surface diseases. *Microsc. Microanal.* **23**, 697–707 (2017).
48. E. Knop, N. Knop, The role of eye-associated lymphoid tissue in corneal immune protection. *J. Anat.* **206**, 271–285 (2005).
49. P. J. Murray, J. E. Allen, S. K. Biswas, E. A. Fisher, D. W. Gilroy, S. Goerdt, S. Gordon, J. A. Hamilton, L. B. Ivashkiv, T. Lawrence, M. Locati, A. Mantovani, F. O. Martinez, J. L. Mege, D. M. Mosser, G. Natoli, J. P. Saeij, J. L. Schultze, K. A. Shirey, A. Sica, J. Suttles, I. Udalova, J. A. van Ginderachter, S. N. Vogel, T. A. Wynn, Macrophage activation and polarization: Nomenclature and experimental guidelines. *Immunity* **41**, 14–20 (2014).
50. R. M. Ransohoff, A polarizing question: Do M1 and M2 microglia exist? *Nat. Neurosci.* **19**, 987–991 (2016).
51. G. Qiu, G. Zheng, M. Ge, J. Wang, R. Huang, Q. Shu, J. Xu, Mesenchymal stem cell-derived extracellular vesicles affect disease outcomes via transfer of microRNAs. *Stem Cell Res Ther* **9**, 320 (2018).
52. T. Thomou, M. A. Mori, J. M. Dreyfuss, M. Konishi, M. Sakaguchi, C. Wolfrum, T. N. Rao, J. N. Winnay, R. Garcia-Martin, S. K. Grinspoon, P. Gorden, C. R. Kahn, Adipose-derived circulating miRNAs regulate gene expression in other tissues. *Nature* **542**, 450–455 (2017).
53. F. Shahjin, S. Chand, S. V. Yelamanchili, Extracellular vesicles as drug delivery vehicles to the central nervous system. *J. Neuroimmune Pharmacol.* **15**, 443–458 (2020).
54. S. Kang, T. Tanaka, M. Narazaki, T. Kishimoto, Targeting interleukin-6 signaling in clinic. *Immunity* **50**, 1007–1023 (2019).
55. F. M. Elahi, D. G. Farwell, J. A. Nolta, J. D. Anderson, Preclinical translation of exosomes derived from mesenchymal stem/stromal cells. *Stem Cells* **38**, 15–21 (2020).
56. D. M. Pegtel, S. J. Gould, Exosomes. *Annu. Rev. Biochem.* **88**, 487–514 (2019).
57. T. B. Abud, F. Amparo, U. S. Saboo, A. Di Zazzo, T. H. Dohlman, J. B. Ciolino, P. Hamrah, R. Dana, A clinical trial comparing the safety and efficacy of topical tacrolimus versus methylprednisolone in ocular graft-versus-host disease. *Ophthalmology* **123**, 1449–1457 (2016).
58. S. Karakus, D. Agrawal, H. B. Hindman, C. Henrich, P. Y. Ramulu, E. K. Akpek, Effects of prolonged reading on dry eye. *Ophthalmology* **125**, 1500–1505 (2018).
59. J. S. Wolffsohn, R. Arita, R. Chalmers, A. Djalilian, M. Dogru, K. Dumbleton, P. K. Gupta, P. Karpecki, S. Lazreg, H. Pult, B. D. Sullivan, A. Tomlinson, L. Tong, E. Villani, K. C. Yoon, L. Jones, J. P. Craig, TFOS DEWS II diagnostic methodology report. *Ocul. Surf.* **15**, 539–574 (2017).
60. L. Guo, P. Lai, Y. Wang, T. Huang, X. Chen, C. Luo, S. Geng, X. Huang, S. Wu, W. Ling, L. Huang, X. Du, J. Weng, Extracellular vesicles from mesenchymal stem cells prevent contact hypersensitivity through the suppression of Tc1 and Th1 cells and expansion of regulatory T cells. *Int. Immunopharmacol.* **74**, 105663 (2019).
61. J.-P. Abbuehl, Z. Tatarova, W. Held, J. Huelsken, Long-term engraftment of primary bone marrow stromal cells repairs niche damage and improves hematopoietic stem cell transplantation. *Cell Stem Cell* **21**, 241–255.e6 (2017).
62. K. Iwai, T. Minamisawa, K. Suga, Y. Yajima, K. Shiba, Isolation of human salivary extracellular vesicles by iodixanol density gradient ultracentrifugation and their characterizations. *J. Extracell. Vesicles* **5**, 30829 (2016).
63. D. Bachurski, M. Schuldner, P. H. Nguyen, A. Malz, K. S. Reiners, P. C. Grenzi, F. Babatz, A. C. Schauss, H. P. Hansen, M. Hallek, E. Pogge von Strandmann, Extracellular vesicle measurements with nanoparticle tracking analysis—An accuracy and repeatability comparison between NanoSight NS300 and ZetaView. *J. Extracell. Vesicles* **8**, 1596016 (2019).
64. P. Lai, X. Chen, L. Guo, Y. Wang, X. Liu, Y. Liu, T. Zhou, T. Huang, S. Geng, C. Luo, X. Huang, S. Wu, W. Ling, X. Du, C. He, J. Weng, A potent immunomodulatory role of exosomes derived from mesenchymal stromal cells in preventing cGVHD. *J. Hematol. Oncol.* **11**, 135 (2018).
65. M. A. Lemp, Report of the National Eye Institute/Industry workshop on clinical trials in dry eyes. *CLAO J.* **21**, 221–232 (1995).
66. C. He, Y. Liu, Z. Huang, Z. Yang, T. Zhou, S. Liu, Z. Hao, J. Wang, Q. Feng, Y. Liu, Y. Cao, X. Liu, A specific $RIP3^{+}$ subpopulation of microglia promotes retinopathy through a hypoxia-triggered necroptotic mechanism. *Proc. Natl. Acad. Sci. U.S.A.* **118**, e2023290118 (2021).
67. C. J. Li, P. Cheng, M. K. Liang, Y. S. Chen, Q. Lu, J. Y. Wang, Z. Y. Xia, H. D. Zhou, X. Cao, H. Xie, E. Y. Liao, X. H. Luo, MicroRNA-188 regulates age-related switch between osteoblast and adipocyte differentiation. *J. Clin. Invest.* **125**, 1509–1522 (2015).

Acknowledgments

Funding: This work was supported by the National Key R&D Program of China (2018YFA0108300), National Natural Science Foundation of China (nos. 81630022, 82070176, and 81900886), and Natural Science Foundation of Guangdong Province, China (no. 2019B151502006). **Author contributions:** X. Liu and C.H. conceived and supervised the work. T.Z., C.H., P.L., Y.L., Z.Y., H.X., and X. Lin performed in vitro and in vivo experiments. T.Z. and B.N. performed bioinformatic analyses. T.Z., C.H., and P.L. collected the clinical data and performed the image processing and data analysis. L.L. enrolled the patients and assisted in the clinical trial. W.Y. assisted in the exosome isolation. C.E.E. guided the flow cytometry. X. Liu, C.H., and C.E.E. wrote the manuscript. R.J. and D.P. revised the manuscript. **Competing interests:** The authors declare that they have no competing interests. **Data and materials availability:** All the raw and analyzed data associated with exosomes miR sequencing have been uploaded to the Gene Expression Omnibus repository (GSE166585). All data needed to evaluate the conclusions in the paper are present in the paper and/or the Supplementary Materials.

Submitted 14 June 2021
Accepted 17 November 2021
Published 12 January 2022
10.1126/sciadv.abj9617